Received: 14 June 2020 | Revised: 7 July 2021 | Accepted: 9 July 2021 | Published on: 29 July 2021

DOI: 10.1002/joc.7299

RESEARCH ARTICLE

International Journal of Climatology RMetS

Impact of a large artificial lake on regional climate: A typical meteorological year Meso-NH simulation results

Maksim Iakunin[1,2] | **Edgar F.M. Abreu**[1] | **Paulo Canhoto**[1] | **Sara Pereira**[1] | **Rui Salgado**[1]

[1]Department of Physics, Institute of Earth Sciences—ICT, University of Évora, Évora, Portugal

[2]Institute of Bio- and Geosciences, Agrosphere (IBG-3) Research Centre Jülich (FZJ) Wilhelm-Johnen-Straße, Jülich, Germany

Correspondence
Maksim Iakunin, Department of Physics, Institute of Earth Sciences—ICT, University of Évora, Rua Romão Ramalho 59, Évora 7000-671, Portugal.
Email: m.iakunin@fz-juelich.de

Funding information
ALOP project, Grant/Award Number: ALT20-03-0145-FEDER-000004; COMPETE 2020 ICT project, Grant/Award Number: UID / GEO / 04683/2019 POCI-01-0145-FEDER-007690; Fundação para a Ciência e a Tecnologia, Grant/Award Number: SFRH/BD/136433/2018; TOMAQAPA, Grant/Award Number: FCT reference PTDC/CTA-MET/29678/2017

Abstract

Large artificial lakes and reservoirs affect the meteorological regime of the shore area and the local climate takes on a number of new features that were previously absent. This work focuses on the weather impact of the Alqueva reservoir, the largest artificial lake in Western Europe. An extensive set of numerical simulations using Meso-NH mesoscale atmospheric model coupled with FLake (Freshwater Lake) scheme was carried out. The simulations covered a 12-month period that was chosen to compose a so-called Typical Meteorological Year. This artificial time period is meant to represent the typical meteorological conditions in the region and the model results are used to assess the changes in the local climate. To evaluate the raw impact of the reservoir, two different scenarios of simulations were compared: (A) with the reservoir as it exists nowadays and (B) without the reservoir using the older surface dataset. The results show decrease of air temperature during daytime (10–9°C) and nighttime increase (up to 10°C). In nearest towns, daily maximum temperature decreased and daily minimum temperature increased, which refers to milder weather conditions. Alqueva mainly showed suppression in fog formation in the nearby area. Local breeze regime was studied and monthly lake/land breezes were described.

KEYWORDS

artificial reservoir, mesoscale atmospheric modelling, typical meteorological year, weather

1 | INTRODUCTION

Inland water bodies, in particular reservoirs, are peculiar living sensors in the weather/climate system of the Earth. Large and deep lakes have a significant impact on regional weather and climate (Samuelsson *et al.*, 2010; Eerola *et al.*, 2014), as shown in well-described examples, such as the Great American lakes (Bates *et al.*, 1993; Scott and Huff, 1996; Notaro *et al.*, 2013). Lakes have a higher heat capacity and thermal inertia and lower surface albedo and roughness length than land surface, which determine their impact on the atmosphere (Bonan, 1995). They interact with the atmospheric boundary layer through momentum, heat and moisture exchange, and their influence on local weather patterns is expressed in diurnal and seasonal variability at various spatial scales

(Choulga *et al*., 2014; Le Moigne *et al*., 2016). Lakes' heat storage and emission cycles are responsible for summer/daytime cooling and winter/night warming effects (Bonan, 1995; Samuelsson *et al*., 2010) and the formation of characteristic features of local breeze patterns (Bates *et al*., 1993; Segal *et al*., 1997). Under certain atmospheric conditions such heat emissions may cause fog formation when cold moist air mass moves over a warmer lake surface. Recent numerical studies showed such effects in lakes and reservoirs, for example, in Chile (Bischoff-Gauß *et al*., 2006), African Great Lakes (Thiery *et al*., 2014), Lake Sobradinho in Brazil (Ekhtiari *et al*., 2017).

The Alqueva reservoir (south-east of Portugal) is the largest artificial lake in Western Europe (surface area of 250 km^2) and it was established in 2002 after the closing of the dam on the Guadiana river. An emergence of such a large water body significantly affected regional environment. The Alqueva reservoir was the object of various multidisciplinary studies, such as ecology and water quality monitoring (Potes *et al*., 2012, 2018; Iakunin *et al*., 2020; Rodrigues *et al*., 2020), biology (Novais *et al*., 2018), land use (Penha *et al*., 2016; Tomaz *et al*., 2017), and meteorology (Lopes *et al*., 2016; Policarpo *et al*., 2017; Potes *et al*., 2017). The aim of this study is to assess the impact of the reservoir on the local regional weather regime using an extensive set of atmospheric simulations. The Meso-NH atmospheric model (Lac *et al*., 2018) was used for that purpose. A previous case study experiment (Iakunin *et al*., 2018) showed that the Meso-NH model successfully represents the meteorological conditions and the local lake effects of the Alqueva reservoir. To capture the long-term meteorological effects of the lake the numerical simulation should cover 16 years (2004–2019) of the Alqueva lifetime, but such experiment would require enormous computing resources and data storage. A reasonable alternative is to make 1-year simulation over a period that is representative of the meteorological conditions of the region. One of the possible methodologies for creating such a period is to build a Typical Meteorological Year.

A Typical Meteorological Year (TMY) is a weather dataset, widely used for energy simulations in buildings and renewable energy systems (Chan, 2016; Abreu *et al*., 2018). This typical year comprises twelve concatenated typical months that are able to reproduce the long-term data statistics and, therefore, are useful to the scope of this work. Although several methodologies have been proposed in the literature to generate typical weather datasets (e.g., Festa and Ratto (1993); Gazela and Mathioulakis (2001)), the most used methodology was presented by Hall *et al*. (1978), known as Sandia method, and it was the methodology used here. Newer versions of this method were developed by the National Renewable Energy Laboratory (NREL), namely the TMY2 (Marion and Urban, 1995) and TMY3 (Wilcox and Marion, 2008). However, their implementation requires direct normal irradiance measurements, which were not readily available during all of the time period under analysis. The Sandia method allowed for TMYs to be reported in the literature for various locations, such as Athens (Pissimanis *et al*., 1988), different climates of Turkey (Pusat *et al*., 2015), distinct places in Madeira Island (Abreu *et al*., 2018) or the Argentine littoral region (Bre and Fachinotti, 2016), to mention a few. A TMY is widely used in renewable energy and building heat balance applications, but has also been used for other climate and environmental studies. In biometeorology, the TMY methodology was applied for greenhouses design (Fernández *et al*., 2015) or to optimize irrigation strategies and assess the atmospheric environmental impact of a combined district heating system (Domínguez *et al*., 2013; Haichao *et al*., 2013; Martínez-Romero *et al*., 2019).

The principal questions of the current study are: to what extent does a reservoir like Alqueva affect the air temperature under such climate conditions, does it increase (or decrease) the amount of fog days in the region, and what are the seasonal breeze patterns associated with the reservoir. The structure of the article is the following. The Introduction is followed by the Data and Methods section, which is dedicated to the specification of the study area, data, models, and the approach used in the work, case study that was made prior to the current work, design of the TMY, and the experiment setup. Section 3 summarizes the results obtained from the numerical simulations and the Discussion part concludes the results, the aim of the work, and possible perspectives.

2 | DATA AND METHODS

2.1 | Study area

The Alqueva reservoir was established in 2002 when the dam gates on the Guadiana river were closed (https://www.edia.pt). The reservoir fills the former river valley in the southeast of Portugal on the Portugal-Spain border and spreads along 83 km (Figure 1a). The lake surface area at the full storage level covers an area of 250 km^2 with a capacity of 4.15 km^3, 3.15 km^3 of which is usable volume under normal operation. This makes it the largest artificial reservoir in Western Europe. The main purpose of the Alqueva reservoir is to provide water supply for domestic use and irrigation and hydroelectric power in the region. The reservoir irrigates about 120,000 ha of agricultural land, ensures water for public supply to

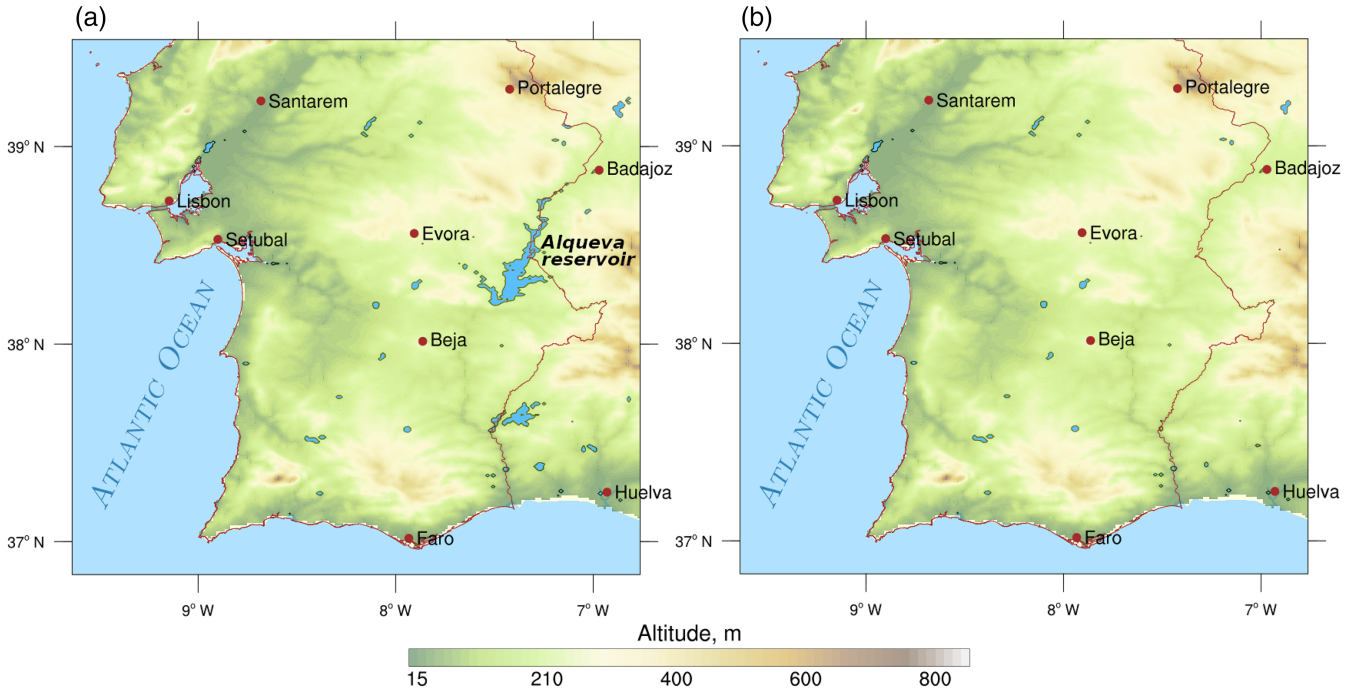

FIGURE 1 The map of working domains used in the simulations. Domain in figure (a) was build with updated surface databases where the Alqueva reservoir is presented and was used in A simulations. Figure (b) corresponds to the domain where the Alqueva was not existed yet B simulations) [Colour figure can be viewed at wileyonlinelibrary.com]

200,000 people and produces enough hydro-electricity to supply a city with more than 500,000 inhabitants.

The Alentejo region, where the Alqueva reservoir is located, is about 1/3 of mainland Portugal. It is known for the irregularity of hydrological resources and long periods of drought (more than 1 year; Silva *et al.*, 2014). According to the Köppen climate classification, the region is characterized by the Mediterranean type of climate, with a small area of the mid-latitude steppe climate.[1] The average daily temperature in summer period is 23°C (June–September), but extreme values may be higher than 45°C. Winter periods are mild and wet, average air temperature is 10.3°C (December–February), although, even in January air temperatures can reach 24°C during long periods of stable anticyclonic conditions. Rain periods are seasonal, normally from October to May. The annual average of accumulated precipitation registered at the climatological station of Beja is 558 mm (1981–2010 normals). Incident solar radiation at the surface is one of the highest in Europe: with mean daily values of about 300 Wm^{-2} and the daily maximum in summer period often reaches 1,000 Wm^{-2}.

2.2 | Models and data

The Meso-NH model (Lac *et al.*, 2018) version 5.4.2 was used for the atmospheric simulations in the present work. It is a non-hydrostatic mesoscale atmospheric model developed by the French research community and is widely used in various atmospheric simulations from synoptic to turbulent scales. Surface-atmosphere interaction is represented using SURFEX scheme version 8.1 (Surface Externalisée, Masson *et al.*, 2013) which is coupled with Meso-NH. The SURFEX scheme includes different surface types (cities, vegetation, etc.), lakes and reservoirs are considered as inland water surfaces and their interaction with atmosphere is simulated by the FLake model (Mironov, 2008; Salgado and Le Moigne, 2010). The FLakemodel is used in numerical weather prediction (NWP), climate modelling, and other numerical prediction systems for environmental applications (http://www.flake.igb-berlin.de/site/applications). It is capable to predict the evolution of the water temperature profile based on the atmospheric forcing data (e.g., air temperature, humidity, shortwave and longwave downwards radiation, wind speed, and pressure) and initial values of mixed layer temperature and depth, bottom temperature, and the thermocline shape factor.

Atmospheric simulations of the current work required the following databases: SRTM (Jarvis *et al.*, 2008) for the surface orography (250 m resolution), ECOCLIMAP II (Faroux *et al.*, 2013) for surface types, HWSD (Harmonized World Soil Database, Nachtergaele *et al.*, 2008) for soil surface textures. For initial conditions and boundary forcing the Meso-NH model used the

European Centre for Medium-Range Weather Forecast (ECMWF) operational analyses.

Water temperature is required to initiate the FLake model (within the Meso-NH simulation or in stand-alone mode). Two past field campaigns held by the ICT (Institute of Earth Sciences), ALEX (ALqueva hydrometeorological EXperiment, 2014, http://www.alex2014.cge.uevora.pt/) and ALOP (ALentejo Observation and Prediction systems, 2017–2019, http://www.alop.ict.uevora.pt/) provide continuous data of water temperature profile measured at a floating platform on the Alqueva reservoir. In addition, water temperature data provided by the EDIA (Empresa de Desenvolvimento e Infraestruturas do Alqueva, a public company that operates the Alqueva Multipurpose Project) were used.

To produce a Typical Meteorological Year, data measured at the observatory of the Institute of Earth Sciences at University of Évora, Portugal (38.57°N, −7.91°E, 290 m a.s.l.) were used. The global horizontal irradiance is measured since 2002 using two Eppley 8–48 ('Black & White') pyranometers with a sample rate of 5 s and 10-min mean values are recorded. Since 2015, a new station was installed at the same location and global horizontal irradiance is measured using a Kipp&Zonnen CM6B pyranometer mounted on a suntracker system. The sample rate of the new data is 1 s and 1-min mean values are recorded.

2.3 | Method

To assess the raw impact of the Alqueva reservoir on local weather and climate an approach based on calculation of differences between two sets of numerical simulations was used. Within this approach two independent sets of simulations were done: the simulations A that correspond to the current surface and real case atmospheric conditions in the study domain, and the simulations B that share all the features with the set A except the surface database in which the Alqueva reservoir does not exist. This can be achieved by using the old versions of the databases that describe the surface (ECOCLIMAP, HSWD, and SRTM) and made before the reservoir was established. As shown in Figure 1, the big difference in the new ECOCLIMAP database is the presence of Alqueva, but other small reservoirs emerged in the south-west of Spain are also taken into account, the largest of which is the Andévalo reservoir. There are also other differences between the two ECOCLIMAP versions, for example, in vegetation related parameters (not shown), that lie within the area of emerged reservoirs. Thus, the differences between the simulations will show essentially the impact of the Alqueva reservoir on atmospheric parameters.

The simulation results are two- or three-dimensional datasets bounded to the chosen model domain. Considering the atmospheric parameter P, we denote P_A and P_B as sets of values of P from the A and B simulations, correspondingly. A derived dataset $P_Y = P_A - P_B$ is called the anomaly of P and corresponds to the 'raw' impact of the Alqueva reservoir. This approach was used for the evaluation of the lake impacts on air temperature and fog formation (low-level clouds). Depending on the result, either positive or negative anomaly on P may be observed (e.g., air temperature becomes higher or lower due to the presence of the Alqueva).

A case study experiment (Iakunin *et al*., 2018) that was conducted earlier used the aforementioned approach. It was aimed on the evaluation of the effects of the Alqueva reservoir under hot summer conditions and description of the breeze circulation induced. The case study covered the dates of 22–24 July, 2014, when intensive atmospheric observations including balloon radiosonde launches were fulfilled in the region in framework of the ALEX project. Validation of simulation results were done by comparison with values observed at the weather stations and floating platform (time series), and measured by radiosondes (vertical profiles). Time series included such atmospheric parameters as wind speed and direction, air temperature, relative humidity, and heat fluxes (latent and sensible). Parameters of vertical profiles were relative humidity, air temperature, and wind speed. Meso-NH showed good representation of the chosen atmospheric characteristics.

The simulation results revealed positive and negative impacts on air temperature and relative humidity due to lake influence and the existing lake breeze circulation. The formation, intensification, and dissipation stages of the lake breeze were documented during the case study. Lake breeze winds might reach 6 $m \cdot s^{-1}$. Daytime lake breeze at the Alqueva reservoir also includes a vertical branch that forces dry air from the altitudes up to 2,500 m to descend to the water surface level.

2.3.1 | Typical Meteorological Year

A TMY consists of 12 concatenated months representing the typical climatological conditions for a particular area. In this work, the TMY is determined using the code developed by Abreu *et al*. (2018) which applies the Sandia method (Hall *et al*., 1978) to find which months better describe the climatological phenomena of a given location. The typical meteorological months selected to be part of the TMY are chosen through the analysis of the following atmospheric parameters: hourly mean, maximum, and minimum values of air temperature and

relative humidity, hourly mean and daily maximum wind speed, and hourly global horizontal irradiance (GHI, 305–2,800 nm) observed over a period of 16 years (2003–2018). The first step on implementing the Sandia method is to determine the cumulative distribution functions (CDF, Equation 1) for both long-term monthly data and each candidate month in each year, for all of the meteorological parameters, using the following equation:

$$CDF_n = \begin{cases} 0 \text{ if } x < x_{(1)} \\ (k-0.5)/n \text{ if } x_k \le x \le x_{k+1} \\ 1 \text{ if } x \ge x_n \end{cases} \quad (1)$$

where n is the number of days for the selected month, x is the value of the meteorological parameter, and k is the ranked order number (k = 1, 2, 3,..., n − 1). Then, the Finkelstein–Schafer (FS) statistics (Finkelstein and Schafer, 1971) are determined using Equation (2), given by:

$$FS = \frac{1}{N}\sum_{i=1}^{N}\delta_i \quad (2)$$

where N is the number of daily records for each month and δ_i is an absolute difference between the long-term and candidate month CDFs. The FS statistics enables comparison between each of the candidate months and the long-term data. To accommodate for different usages of the TMY, a weighted sum (WS) of the FS statistics is determined using specific statistical weights according to the meteorological parameter in question. The statistical weights used in this study, as stated in the Sandia method (Hall *et al*., 1978), are the following: 1/24 for maximum and minimum air temperature and relative humidity, 2/24 for mean air temperature, mean relative humidity, and mean and maximum wind speed, and 12/24 for GHI. Therefore, the WS is given by:

$$WS = \sum_{j=1}^{9}\omega_i FS_j \quad (3)$$

where ω_j is the statistical weight of the meteorological parameter j. The years of the dataset are then sorted in ascending order according to its WS value, and the 5 years with lowest WS are selected as candidate years to be part of the TMY, for each one of the calendar months. The strict implementation of the Sandia method would require the evaluation of the persistence of the global solar irradiance and mean air temperature through the frequency and length of runs of consecutive days with values above and below fixed percentiles. However, a widely used simpler procedure proposed by Pissimanis *et al*. (1988) was followed here in which the GHI is analysed. The deviations of the monthly mean values of GHI with respect to the long-term values for the candidate years are determined using hourly GHI measurements and the root mean square difference statistical indicator given by:

$$RMSD_y = \sqrt{\sum_{g=1}^{Q}\left(GHI_{y,g} - \bar{GHI}_g\right)/Q} \quad (4)$$

where Q is the sunshine duration, $GHI_{y,g}$ is the hourly GHI average for year y and hour g and GHI_g is the long-term GHI mean at hour g. To get 1 year of the five candidate years selected using WS the years that have $RMSD_y > min(RMSD_y)$ + 0.02 kWh·m^{-2} were excluded. If more than one candidate year remained, the years that have $FS_{GHI} > min(FS_{GHI})$ + 0.03 were excluded. If there were still more than one candidate year, the year with lower FS mean temperature was selected. Applying this procedure for each one of the calendar months results in the TMY presented in Table 1). More information on the generation of TMY can be found in the work of Abreu *et al*. (2018).

The validation of the years selected to be part of the TMY is usually carried out by comparison between the monthly mean values of the long-term dataset and the year selected to be part of the TMY (e.g., [Abreu *et al*., 2018; Pusat *et al*., 2015]), as shown in Figure 2.

From Figure 2, it is possible to see how the statistical weights used in Equation (3) affect the comparison between the monthly means of the long-term and TMY data. Higher statistical weight results in higher proximity between the monthly means, as can be seen for the GHI comparison. Nonetheless, the monthly means of the TMY agree well with the long-term means for all meteorological parameters, which means that the TMY accurately characterizes the meteorological phenomena of the time period analysed here (2003–2018) in a single year of real measurements.

TABLE 1 Typical meteorological year used in present work

Month	Year	Month	Year
January	2018	July	2014
February	2006	August	2007
March	2017	September	2011
April	2008	October	2008
May	2005	November	2004
June	2010	December	2018

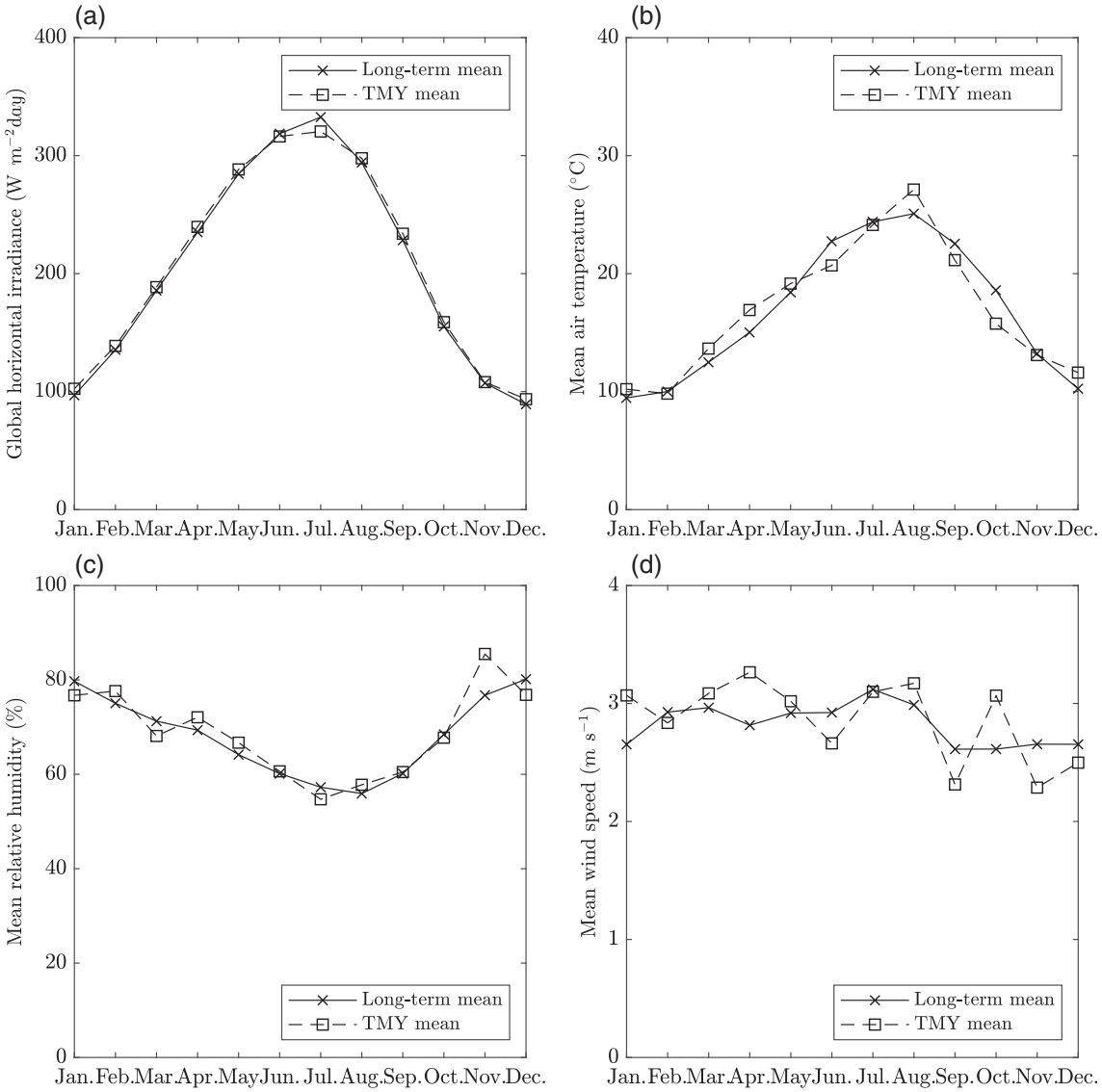

FIGURE 2 Monthly mean values comparison between TMY and long-term data for global horizontal irradiance, mean air temperature, relative humidity, and wind speed

2.3.2 | Experimental setup

The domain that was used for the present atmospheric simulation (Figure 1) is constrained within the rectangle between (36.8329; 39.5419°N) and (−9.63758; −6.76242°E). It consists of 200 × 240 grid pixels with horizontal resolution of 1.25 km, which allows Meso-NH to resolve convection explicitly. Such dimension covered southern part of Portugal, south-west of Spain, and coastal area of the Atlantic Ocean to ensure that the model would properly account for the large-scale maritime influence. There were 70 vertical levels in the domain (up to 23,886 m), 35 of which were below 2,000 m.

The simulations were performed on a single domain, dispensing the use of grid nesting, initialized and forced directly from the European Centre for Medium-Range Weather Forecast (ECMWF) operational analysis, updated every six hours. This practice has been used recently by other authors in studies with Meso-NH (e.g., Jiménez *et al.* (2019); Reinares Martínez *et al.* (2020). As argued by Capecchi and Buizza (2019), this is a pragmatic, low CPU cost, approach to take full advantage of increased resolution of large-scale models and to remove the need for any intermediate grid with the potential benefits outlined in Marsigli *et al.* (2014), namely, that of avoiding the gray zone, where the convection is partially resolved.

During the period covered by the TMY, the horizontal resolutions of the ECMWF operational high resolution analysis were the following: 9 km after March 16, 2016 km between January 2010 and March 2016, and

25 km prior to 2010. Thus, it is likely that the simulations for months prior to 2010 will be affected by a higher error. However, it should be noted that the objective of this work is not to characterize the climate in an absolute way, but rather to assess the impact of a reservoir on local climate based on calculation of differences between two sets of numerical simulations. It was assumed that the errors and limitations introduced by the direct use of operational analyses to initialize and force simulations in a single domain will be approximately the same in both sets of experiments.

According to the chosen method described above, the Meso-NH model was set up for two (*A* and *B*) twelve months simulations. To keep the simulation close to the meteorological large-scale analysis, each month, in turn, was split into ten series of three days runs (except February, which was split into nine series). Three days model run was used earlier in the case study and showed good results in validation. With such an approach, model surface parameters are forced towards analysed values, creating a better conditions for a more accurate representation of the boundary layer. Thus, 238 model runs were made in total (for *A* and *B* experiments: 9 for February and 10 for each other month). Each simulation had a 6 hr spin-up period, so, every model run covered 6 + 72 hr.

The setup configuration included a turbulent scheme based on a 1D closure and the mixing length was computed according to Bougeault and Lacarrere (1989) (BL89). The BL89 is the recommended scheme for mesoscale kilometric scales (e.g., Verrelle *et al.*, 2015). For clouds and explicit precipitation, a mixed-phase microphysical scheme (Cohard and Pinty, 2000; Cuxart *et al.*, 2000) was used. Radiation transfer equations for longwave and shortwave are solved for independent vertical columns (Hogan and Bozzo, 2018). The following parametrizations were taken into account for atmosphere-surface exchanges: Interface Soil Biosphere Atmosphere (ISBA) model (Noilhan and Mahfouf, 1996) for the surface soil and vegetation; the city landscape energy balance was handled according to Masson (2000). The chosen horizontal resolution of 1.25 km allows the explicit resolving of deep convection while shallow convection should be parametrized. The following schemes were used (see Table 2): EDKF (Pergaud *et al.*, 2009), WENO (Lunet *et al.*, 2017), and ICE3 (Pinty and Jabouille, 1998). In the experiment *B* on lake locations ISBA model was running while in the experiment *A* FLake scheme was applied to the lake areas. Figure 3 shows land cover types according to ECOCLIMAP II database for the experiment *B* at the Alqueva area. Calculation time step was set to 30 s, radiation scheme was executed every 300 s in case of clear sky and every 60 s in cloudy conditions.

Initial values for the FLake scheme variables (surface and bottom water temperature, mixed layer depth, and shape function of the thermocline) were obtained from the observations that were made during the ALOP (2017–2019) and earlier ALEX (2014) field campaigns. These experiments included continuous measuring of water temperature profile at the floating platform which was enough for the simulations of three months (January 2018, July 2014, and December 2018) of the TMY. For the other TMY months, however, measurements of the water temperature profile were not available. To provide the Meso-NH—FLake with realistic initial water temperature profiles, series of preliminary FLake-standalone simulations were made. It was shown earlier that the FLake standalone model is capable of representing water temperature profile in Alqueva quite accurately (Iakunin *et al.*, 2020). The atmospheric data used to force FLake offline runs were obtained from the ECMWF analysis

TABLE 2 Meso-NH physical schemes used in the numerical experiment

Feature	Scheme name
Deep convection	—
Shallow convection	EDKF
Turbulance	BL89
Radiation transfer	EcRad
Advection	WENO
Clouds	ICE3

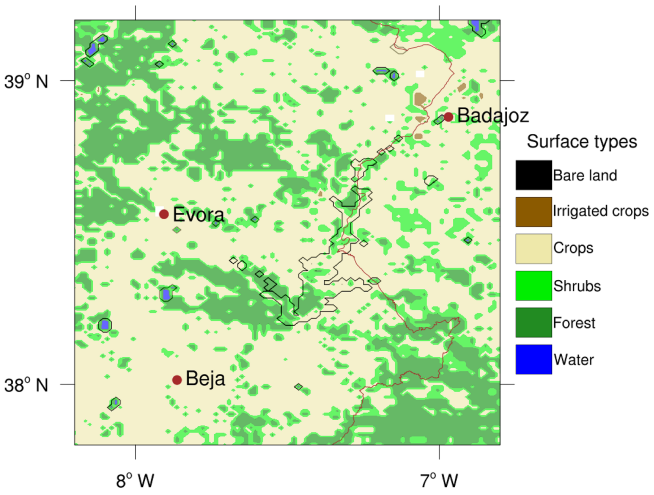

FIGURE 3 Land cover types in the area of interest prior to the emergence of the Alqueva according to ECOCLIMAP II database. Black contours correspond to the Alqueva and other small lakes borders [Colour figure can be viewed at wileyonlinelibrary.com]

with satisfactory time resolution (3 hours), while data from the reservoir management company, EDIA, were used to initialize the water surface temperature. Taking into account the fact that bottom temperature does not vary much in a given month from year to year, the average monthly bottom temperature value from the ALOP observations was used. To minimize the traces of the initial uncertainties in the required data, each preliminary simulation included one-month spin-up period.

For example, to obtain the FLake input parameters for February 2006, a standalone FLake 2-months simulation starting in January was performed. The surface water temperature from the EDIA observations and mean January bottom temperature were used as initial conditions, and ECMWF data as atmospheric forcing. A month for a model spin-up highly reduces the uncertainties of the initial values, so the February data could be used as a realistic input for each Meso-NH further simulation.

2.4 | Validation

Before proceeding with analysis of the reservoir's impact on weather, it is important to assess the quality of Meso-NH simulation over the TMY by comparing the results against reference data from weather stations and ECMWF ERA5-Land reanalysis.

Three weather stations located in Évora, Mitra, and Portel provided hourly observations of air temperature, relative humidity, wind speed, and downwelling shortwave radiation to verify Meso-NH simulations through all months of the TMY. The choice of those stations is motivated by the following conditions: these are the closest weather stations to the Alqueva reservoir and they provide complete time series of observations that cover the whole simulation period. Figure 4 compares the hourly values of the selected variables at the weather station sites. A good comparison of the model values to the observations is presented, especially for air temperature and shortwave radiation, for which the linear fit of hourly values is close to the one-to-one line and the correlation coefficients are .97 and .94, respectively. Station and monthly averaged biases, mean absolute errors (MAE), and root mean square errors (RMSE) for data comparison against weather stations are presented in Table 3. Although a small constant overestimation of shortwave radiation (26 Wm^{-2}) and underestimation of relative humidity (10% during the TMY) is observed, the overall quality of reproduction of atmospheric parameters by Meso-NH is high.

Monthly averaged data of 10 m wind components, 2 m air temperature, surface level pressure and downwelling shortwave radiation obtained by Meso-NH for the TMY was compared against ECMWF ERA5-Land reanalysis. Combining model data with observations from all over the world, this reanalysis dataset provides a consistent view of the evolution of land variables over several decades at a resolution of $0.1 \times 0.1°$ (Muñoz, 2019). Monthly-mean averaged data used in the current work is a post-processed subset of the full ERA5-Land dataset. Meso-NH 1-hour outputs of 1.25 km horizontal resolution were monthly averaged and regridded to ERA5 9-km grid. Then, a sea mask was applied to both ERA5-Land and Meso-NH outputs. After this procedure it was possible to directly compare two datasets by subtracting ERA5 from Meso-NH field by field, results of which are presented in Table 4. A slight underestimation of Meso-NH data on air temperature (−1°C) and atmospheric pressure (−1.47 hPa) can be noticed. At the same time, the shortwave radiation is slightly overestimated by a value similar in magnitude (19 Wm^{-2}) to that which was obtained when comparing with the stations. It is worth noting the excellent comparison to the wind speed components of the reanalysis data with yearly MAE of 0.4 $m{\cdot}s^{-1}$.

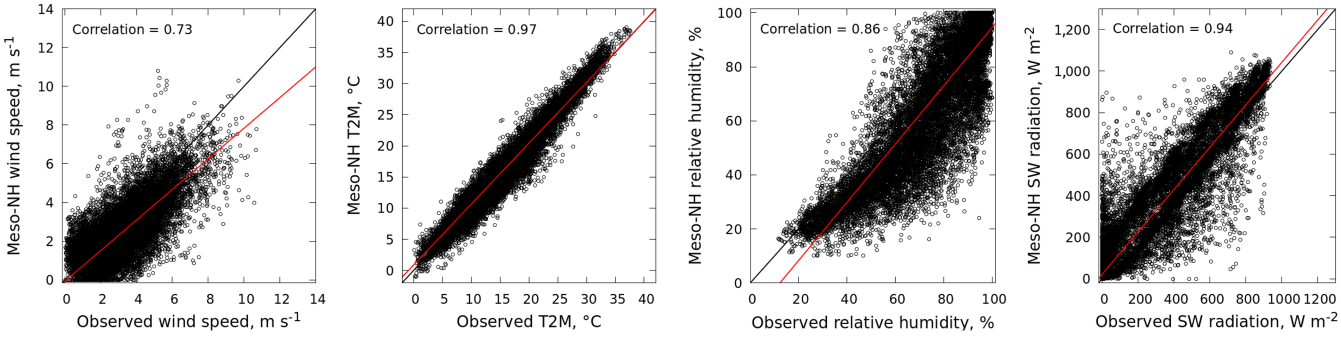

FIGURE 4 Scatterplots comparison of the TMY hourly 2 m air temperature, relative humidity, wind speed, and downwelling shortwave radiation between observations and Meso-NH simulation data at Evora (38.5679°N, −7.9115°E), Mitra (38.5292°N, −8.0169°E), and Portel (38.3092°N, −7.7030°E) sites. One-to-one lines and the least-squared fit through all data points are plotted with solid black and red lines, respectively [Colour figure can be viewed at wileyonlinelibrary.com]

TABLE 3 Statistic results of the comparison of TMY monthly mean wind speed, 2 m air temperature, relative humidity, and shortwave radiation between observations at weather stations and Meso-NH simulation data

	Wind speed, $m \cdot s^{-1}$			T2M, K			Relative humidity, %			SWR, $W \cdot m^{-2}$		
	Bias	*MAE*	*RMSE*	*Bias*	*MAE*	*RMSE*	*Bias*	*MAE*	*RMSE*	*Bias*	*MAE*	*RMSE*
January	−0.7	1	1.2	0.7	1.3	1.6	−7	10	13	28	39	77
February	−0.4	1	1.3	0.8	1.2	1.5	−14	16	19	27	44	87
March	−0.6	1	1.3	0.7	1.4	1.7	−6	11	15	32	62	116
April	−0.8	1.1	1.5	−0.1	1.4	1.8	−16	17	20	35	62	118
May	−0.7	1	1.2	0.9	1.4	1.9	−24	24	25	12	79	132
June	−1	1.3	1.6	0	1.5	1.9	−6	10	12	35	65	111
July	−0.5	1.1	1.4	0.3	1.2	1.5	−4	8	9	36	67	106
August	−0.7	1.1	1.4	0.2	1.1	1.5	−7	9	11	19	51	86
September	−1	1.2	1.5	−0.6	1.5	1.9	−5	8	10	30	58	104
October	−0.7	1	1.3	0	1.4	1.8	−14	15	17	17	43	85
November	−0.4	0.9	1.1	1.1	1.4	1.7	−27	27	29	3	37	75
December	−0.2	1	1.2	0.8	1.4	1.8	−6	9	12	25	35	70
Year	−0.7	1.1	1.3	0.4	1.3	1.7	−10	12	15	26	53	97

3 | RESULTS

3.1 | Air temperature

To evaluate the impact of Alqueva on the 2 m air temperature (T2M), we calculated daily maximum and minimum of $T2M_Y$ (i.e., positive and negative anomalies), and then composed monthly average values. The results are shown in Figure 5. Positive $T2M_Y$ happens during the nighttime, when the water temperature is higher than the surrounded land. The highest values of positive anomalies occur over the reservoir normally close to sunrise. Negative anomalies, on the contrary, appear mostly during day time, frequently cole to the time of the maximum daily temperature. Over the land, lake impact on air temperature follows the dominant winds in the area. West winds prevail during the nights of the warm season (from March to September) due to the large-scale sea breeze circulation, and the negative temperature anomaly may stretch over 15–20 km to the east but their values rarely exceed 1°C. Cold season nights (October–February) are characterized by north and north-west dominant winds, so the corresponding positive anomalies (+1°C) spread to the south direction up to 20 km and the valley relief of that area contributes to this. Near the lake shores (within the area of less than 5 km), these anomalies usually reach +1.5°C.

Figure 6 shows extreme values of positive and negative T2M anomalies over the whole TMY and the 90th percentile of the daily minimum and maximum anomalies. Positive anomalies cover larger area and can be observed much farther from the reservoir in all directions, especially in the south and southwest. They might reach up to +5°C over land and up to +10°C over the water surface of the reservoir. Negative temperature anomalies are more local and usually rarely observed far from the lake shore, although, they might be equally strong, reaching −4°C over surrounding land and −9°C above the lake surface.

To assess how Alqueva affects daily temperature in nearby locations, four towns were chosen: Moura (7 km east of the reservoir), Mourão (1 km southeast of the reservoir), Pedrogão (15 km southwest of the reservoir), and Reguengos de Monsaraz (12.25 km northwest of the reservoir). Each town was represented by 9 grid points. Fraction of water in them was 0 and the fraction of urban land was 0.1 (Moura), 0.07 (Mourão), 0.006 (Pedrogão), and 0.136 (Reguengos de Monsaraz). Location of the chosen towns are shown in Figure 7. In this case, we examined how maximum and minimum daily temperatures have changed (Figure 8). Mourão, the closest town to the Alqueva, is more affected by the daily temperature impact, as the monthly mean maximum daily temperature decreased by 0.3–0.4°C in October–April, and up to 0.6°C in July–September. Monthly mean daily minimum temperature, on the contrary, increased by 0.5–1.0°C during the whole TMY (Figure 8 a, b). In Moura, which is located 7 km east of the Alqueva, the temperature impact is much weaker. During the TMY, the maximum daily T2M has not decreased more than 0.3°C (in December) and minimum daily T2M slightly increased by ∼0.4°C in October–November, while the anomalies during the rest

TABLE 4 Statistic results of the comparison of the domain area averaged TMY monthly mean wind speed components, 2 m air temperature, surface level pressure, and shortwave radiation between ECMWF ERA5-Land reanalysis and Meso-NH simulation data

	U10, $m \cdot s^{-1}$			V10, $m \cdot s^{-1}$			T2M, K			Press, Pa			SWR, $W \cdot m^{-2}$		
	Bias	*MAE*	*RMSE*	*Bias*	*MAE*	*RMSE*	*Bias*	*MAE*	*RMSE*	*Bias*	*MAE*	*RMSE*	*Bias*	*MAE*	*RMSE*
January	0.0	0.3	0.4	0.2	0.5	0.6	−1.3	1.3	1.3	−143	357	522	5	6	6
February	0.1	0.3	0.4	0.1	0.4	0.5	−1.0	1.0	1.1	−108	351	509	13	13	14
March	0.1	0.3	0.3	0.1	0.3	0.4	−1.1	1.1	1.2	−150	353	516	20	20	21
April	0.3	0.5	0.6	0.2	0.3	0.4	−0.9	0.9	1.0	−194	357	525	29	29	29
May	0.1	0.3	0.4	−0.1	0.4	0.5	−1.1	1.2	1.3	−140	346	506	34	34	34
June	0.5	0.6	0.7	0.2	0.5	0.7	−1.0	1.0	1.1	−150	343	502	34	34	34
July	0.4	0.5	0.6	0.0	0.4	0.5	−0.5	0.6	0.8	−125	338	493	25	25	25
August	0.2	0.4	0.5	−0.2	0.5	0.6	−0.7	0.8	0.9	−155	341	500	22	22	23
September	0.2	0.4	0.4	0.2	0.4	0.5	−0.7	0.8	0.9	−148	341	500	18	18	19
October	0.0	0.3	0.4	−0.1	0.5	0.6	−0.8	0.8	0.9	−160	349	512	19	19	20
November	0.0	0.4	0.5	0.0	0.4	0.6	−1.4	1.4	1.5	−126	350	509	10	10	11
December	0.0	0.3	0.4	0.0	0.4	0.5	−1.4	1.4	1.5	−166	359	526	3	4	5
Year	0.2	0.4	0.5	0.0	0.4	0.5	−1.0	1.0	1.1	−147	349	510	19	20	20

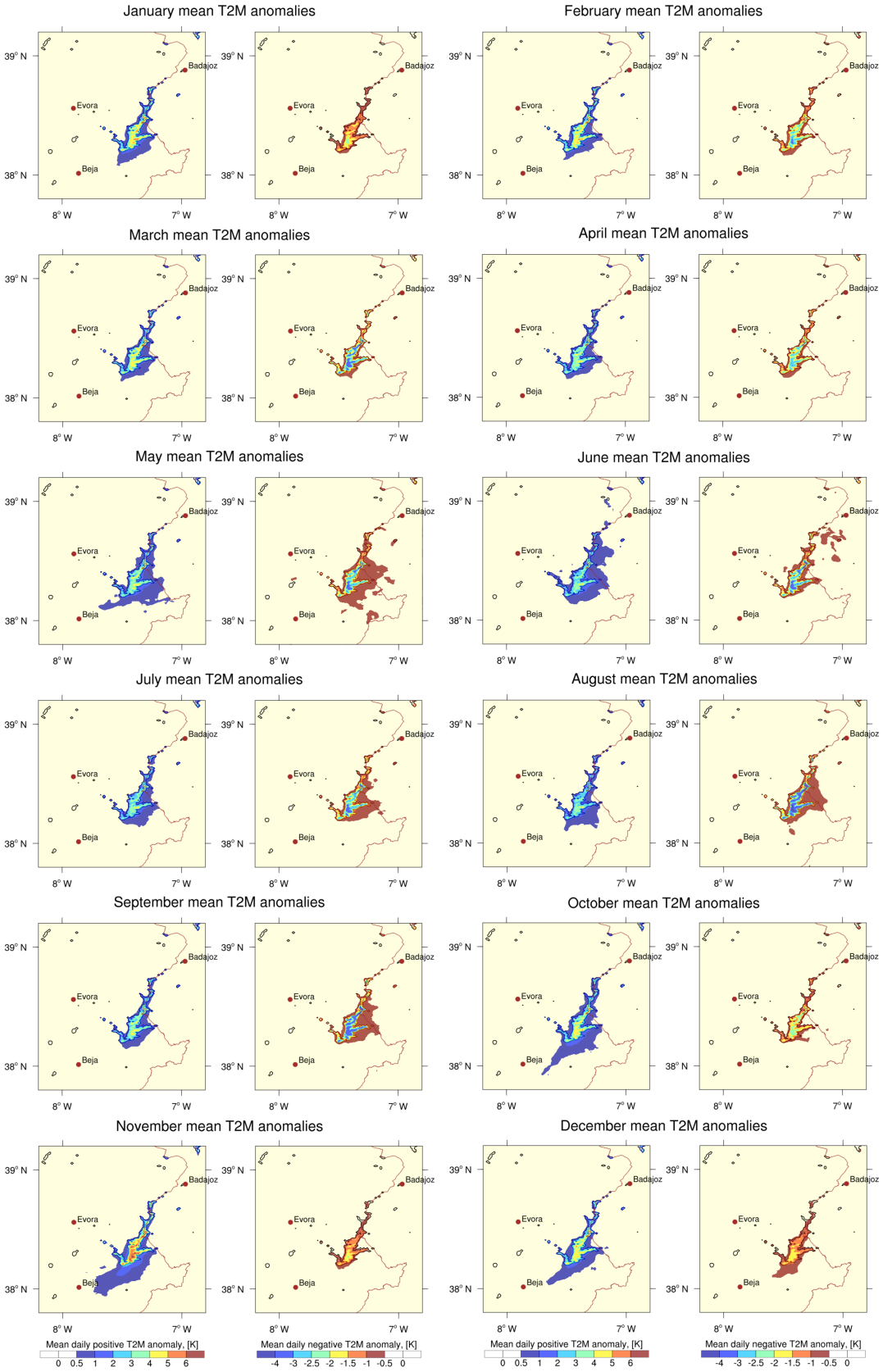

FIGURE 5 Alqueva impact on 2 m air temperature: seasonally averaged maximum positive and negative daily anomalies [Colour figure can be viewed at wileyonlinelibrary.com]

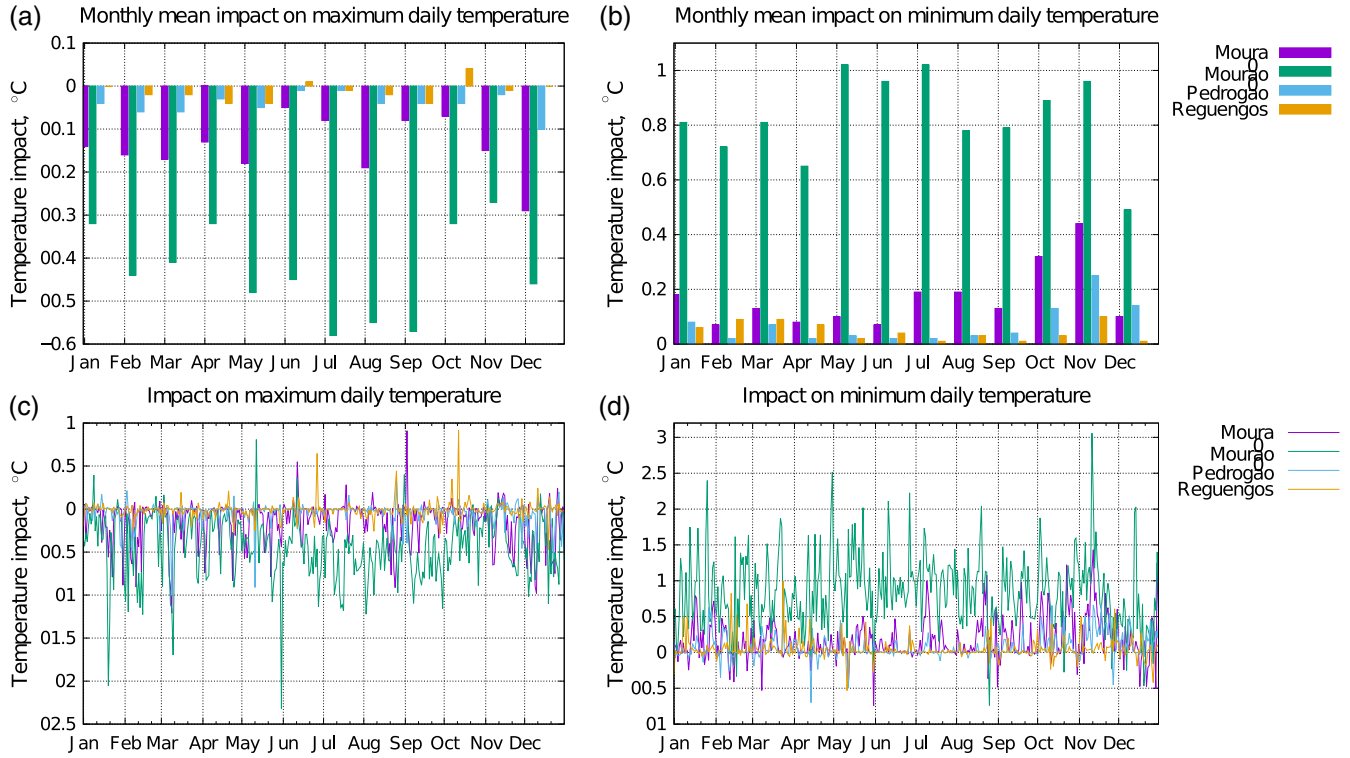

FIGURE 6 Minimum and maximum daily temperatures changes in chosen towns: monthly mean (a,b) and daily (c,d) values [Colour figure can be viewed at wileyonlinelibrary.com]

of the months were not higher than 0.2°C. In Reguengos de Monsaraz and Pedrogão the impact on daily temperature amplitude was quite insignificant due to the distance from the reservoir.

Daily lake impacts on maximum and minimum air temperature shown in Figure 8c,d (c, d), however, can be much higher. In Mourão, maximum daily temperature can increase by up to 0.8°C, and decrease by 2.2°C. In the town of Reguengos, which is the least affected among all, minimum and maximum daily temperatures can even increase by 0.9°C, although such cases are rare.

3.2 | Fog

The impact of the Alqueva reservoir on fogs occurrence was studied using the cloud fraction parameter (CLDFR) at the first atmospheric level. Figure 9 shows a seasonally accumulated values of the $CLDFR_Y$ anomalies. Negative values of this variable indicate the lack of fog due to the presence of the reservoir, while positive values indicate the fog that appeared because of the Alqueva. According to the Meso-NH simulation results, the dominant reservoir impact on fog is negative: the reservoir suppresses the formation of fog. This effect is more visible during winter months of the TMY, with more than 130 of 'fogless' hours registered in December. This number decreases when nights become warmer and during the summer (June–August) Alqueva's impact on fog formation is insignificant.

In annual terms, the simulation results indicate a negative impact on the number of hours of fog mainly over the reservoir, both at night and in the morning. As shown in Figure 10, the reservoir annually suppresses up to 240 hr of fog during nighttime and more than 120 hr in daytime. The suppression is almost over the water due to an increase of the surface and near-surface air temperature. On the other hand, the increase in water vapour due to lake evaporation causes some positive impacts on the neighbourhood. According to the model results shown in Figure 10, the presence of the reservoir contributes to an increase of up to 30 hr of fog per year during night in areas that can be a few tens of kilometres away from the water mirror. During morning, the model indicates the occurrence of positive anomalies of the same order of magnitude over the lake and in neighbouring areas.

Despite statements by local residents who say that there are much more foggy days since the reservoir was established, the simulations suggest only few hours of positive impact per month during the TMY. A detailed analysis shows, however, that under specific atmospheric conditions, there may be a significant positive impact on fog. Dates 19 and 20 of December are two extreme

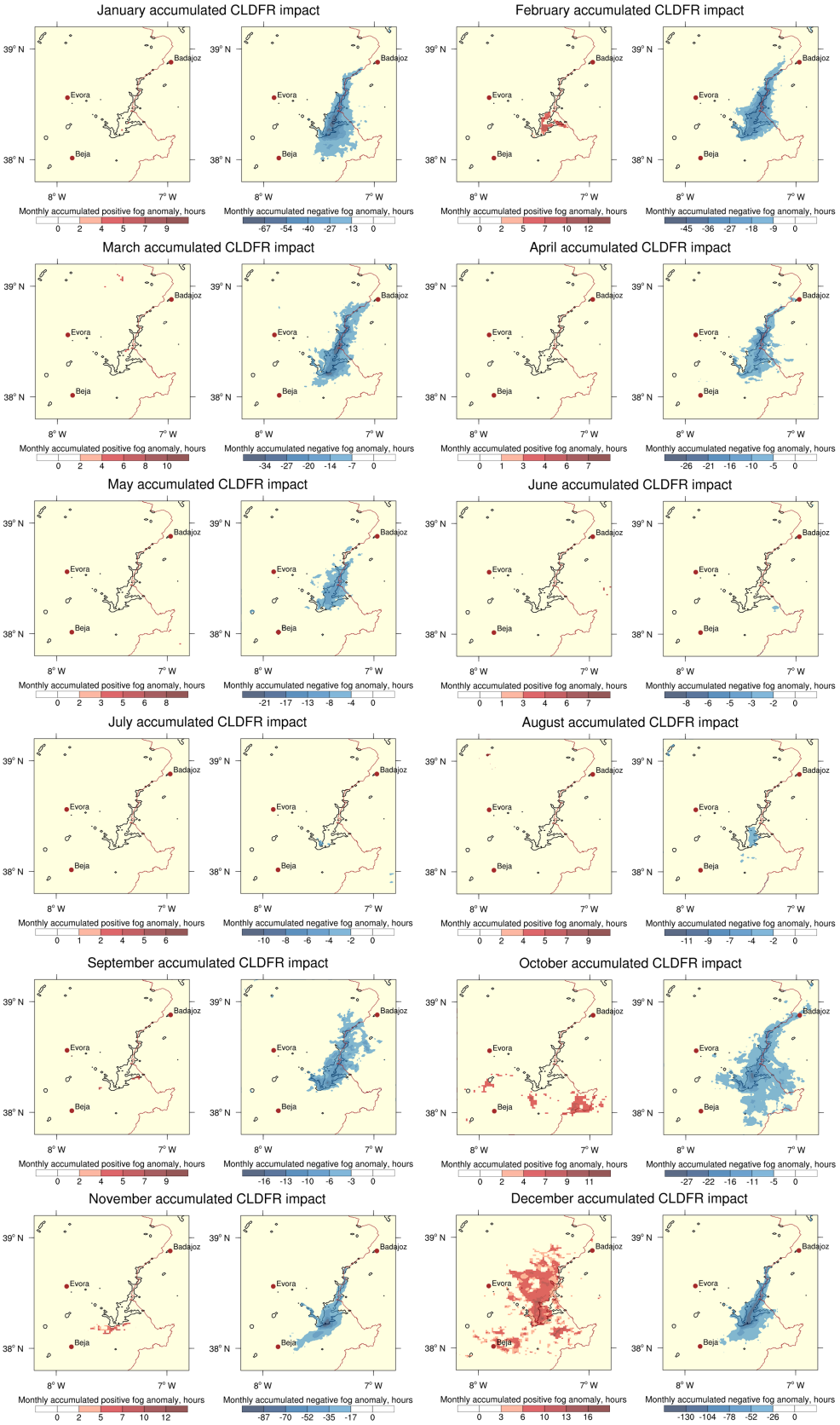

FIGURE 7 Alqueva impact on fog formation: monthly accumulated cloud fraction at 10 m anomalies [Colour figure can be viewed at wileyonlinelibrary.com]

examples of a very strong positive fog anomalies (Figure 11). The simulation showed that a day before these events a very cold weather was observed which led to a strong negative temperature anomaly. In the afternoon of 19 December warm air mass moved from the southeast and was cooled by the cold air above and near

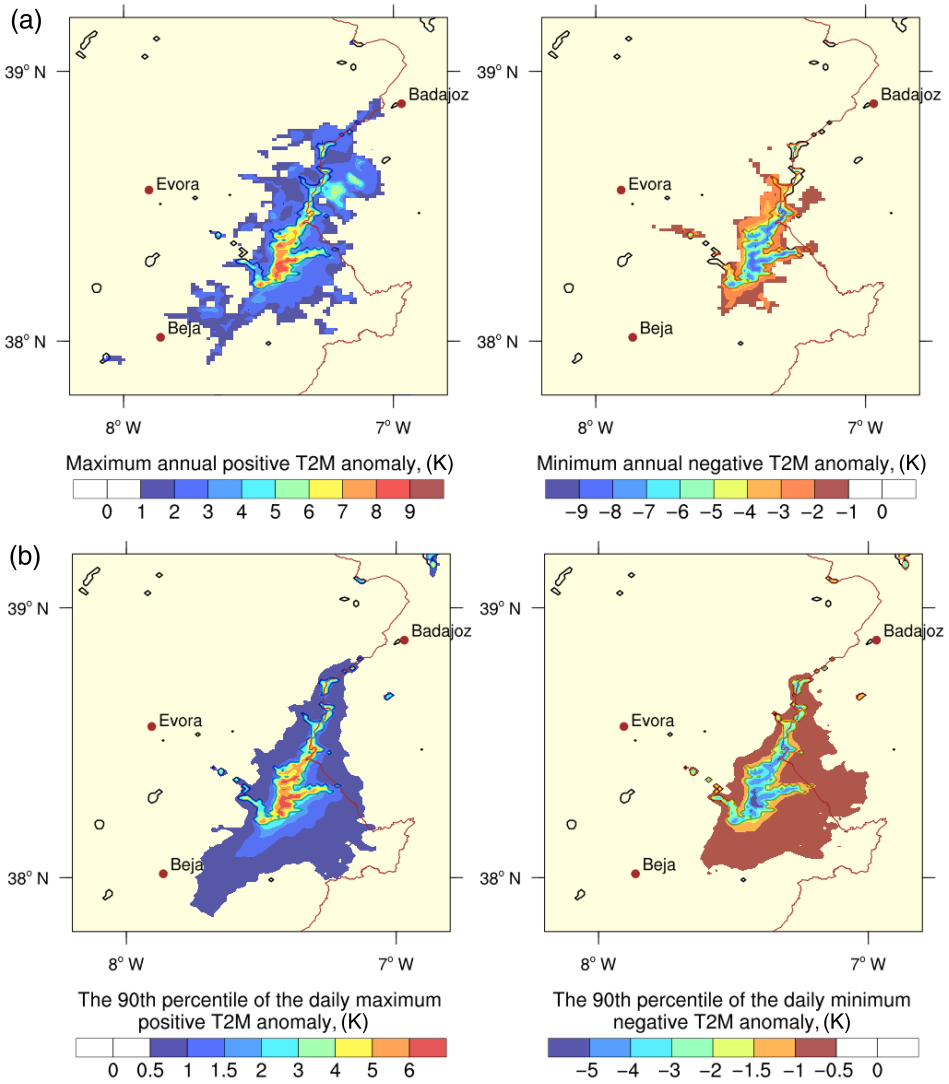

FIGURE 8 Extreme values of T2M anomalies over the TMY (a) and the 90th percentile of the daily minimum and maximum anomalies (b) [Colour figure can be viewed at wileyonlinelibrary.com]

the Alqueva resulting in fog formation. Clouds up to 300 m in altitude were forming over the water surface and shore area of the Alqueva in the afternoon during these days. They were growing and moving in north and northwest direction on the distance of 50–60 km and dissipated by midnight. Although such strong positive impact occurred during the TMY, it may happen in other months which are not typical, since the TMY is not suitable to represent rare/extreme conditions. As pointed out Bergot and Lestringant (2019), it should be noted that numerical prediction of fog remains a challenge due to a whole set of factors, including small-scale processes, complex mesoscale circulation or microphysical processes.

3.3 | Breeze

To study the lake breeze in the current work, three pairs of points on opposite shores of the reservoir were chosen (A/A', B/B', C/C', Figure 7). We assume the breeze system (lake breeze with wind blowing from the lake or land breeze with wind blowing from the land) overlaps the synoptic conditions when the wind directions are opposite in the pair of the chosen points. As an example, for the lake breeze in the A/A' pair of points, the following conditions were applied: wind direction at A point between 45° and 165° and at A' between 195° and 350°. Arithmetic conditions for each pair are listed in Table 5. As an additional condition an angle between two wind vectors should be higher than 60°. These conditions are graphically depicted as ring sectors around the chosen points in Figure 7. An annual regime of the lake and land breezes (average of three pairs of points) is illustrated in Figure 12.

Lake breeze occurs due to the thermal contrast when air above the water surface is colder than the air over the surrounding land. When such conditions are established, the wind starts to blow from the lake to the shores. Warm period of the TMY (June–October) can be considered as a daytime breeze season with 10–15 days of registered

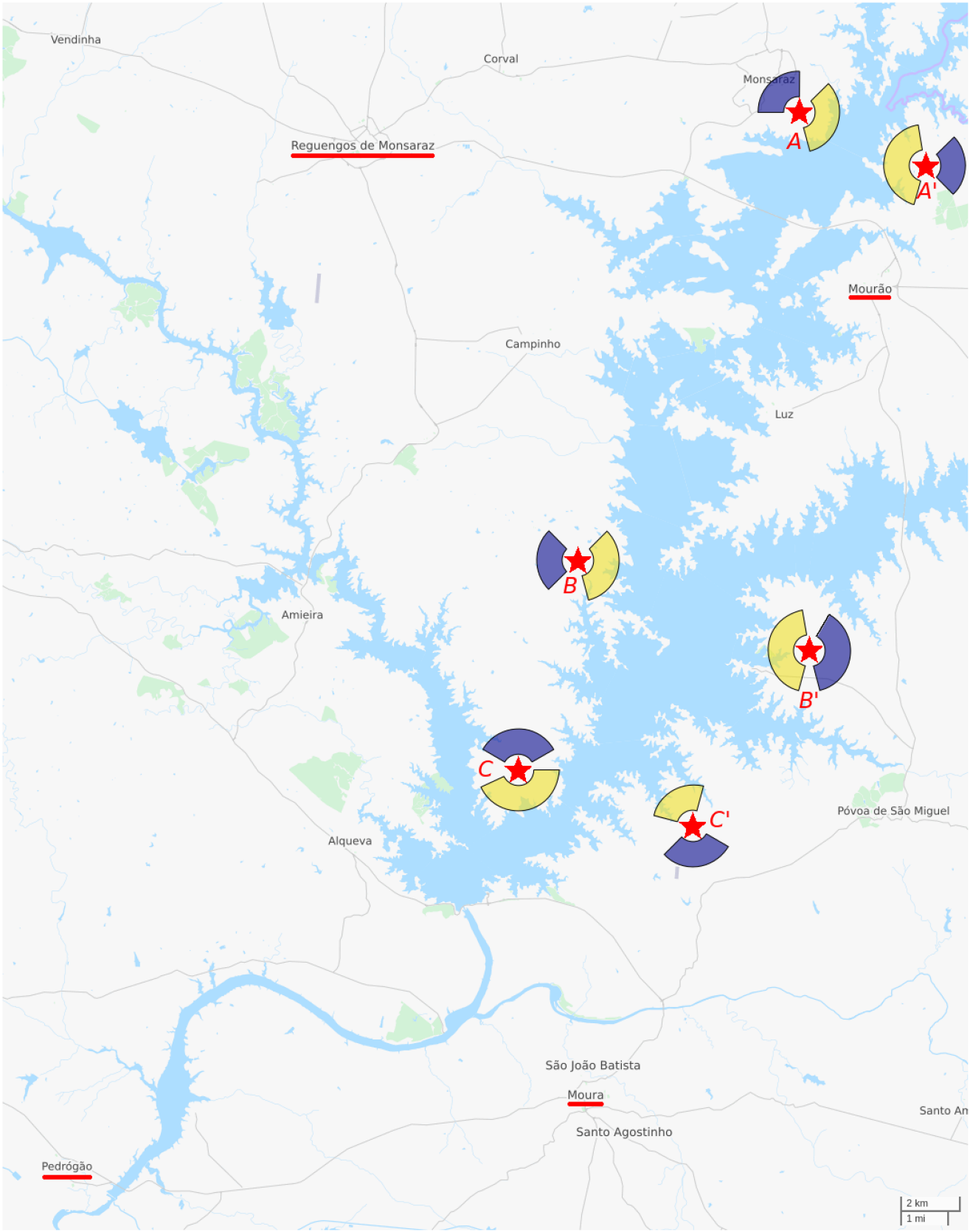

FIGURE 9 Location of the chosen towns (marked with red line) relative to the Alqueva reservoir. Stars mark the points of wind direction study. Yellow and blue ring sectors correspond to the conditions of the lake and land breeze, respectively (©OpenStreetMap contributors) [Colour figure can be viewed at wileyonlinelibrary.com]

breeze (Figure 12a). Counting the amount of hours when the breeze was registered, June, July, and September hold the record, with more than 40 hr of breeze each month (Figure 12b). During the cold period of the TMY, favourable conditions for breeze occur less frequently: 8–10 days in February and March and only 6–7 days in

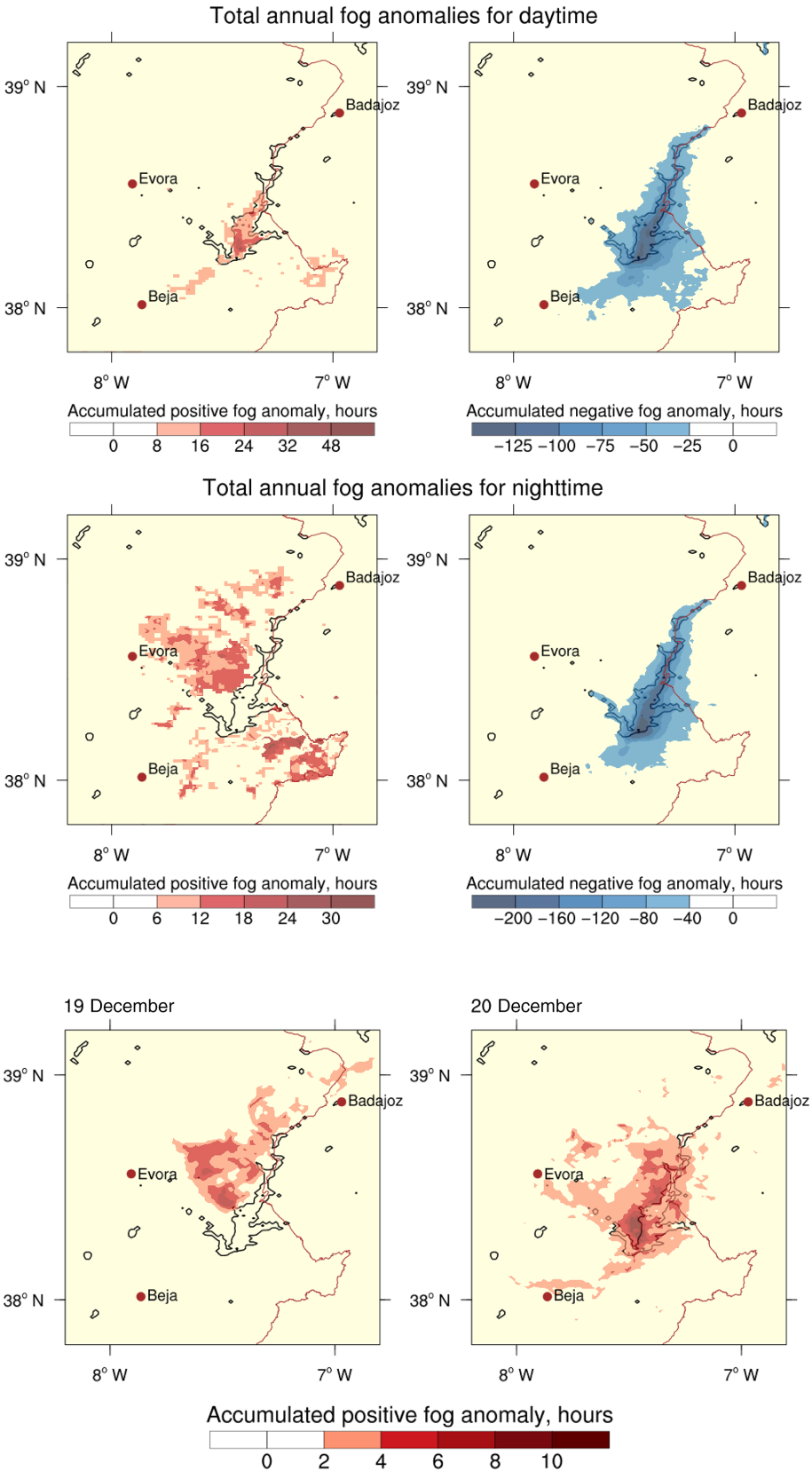

FIGURE 10 Alqueva impact on fog formation: TMY accumulated cloud fraction at 10 m anomalies for day (07–18 UTC) and night (19–06 UTC) time [Colour figure can be viewed at wileyonlinelibrary.com]

FIGURE 11 Cases of the strong positive fog anomalies registered in 19 and 20 of December [Colour figure can be viewed at wileyonlinelibrary.com]

TABLE 5 Ranges of wind direction set to determine lake and land breeze at chosen pairs of points

	Lake breeze	Land breeze
A	[45°; 165°]	[270°; 360°]
A′	[195°; 350°]	[45°; 135°]
B	[45°; 165°]	[225°; 315°]
B′	[195°; 350°]	[30°; 165°]
C	[110°; 240°]	[300°; 60°]
C′	[290°; 10°]	[135°; 225°]

April, November, and December. Calculating an average time of when daytime breeze conditions have occurred, we see almost an annual cycle with maximum in August, when, on average, breezes lasted for 3.5 hr (Figure 12c). In this case, January is an exception: rare breeze days happened in this month revealing quite sustained winds. It is worth noting that in the pair of *B*/*B′* points (the most wide part of the Alqueva reservoir), 20 days of breeze were observed in September.

Land breeze, on the contrary, occurs when the air over the water is warmer than over the land. In this case, wind is blowing towards the lake surface. At the Alqueva reservoir, land breezes were registered more often during the cold months, in January and December (Figure 12a). The number of land breezes is minimal during the summer. At the *C*/*C′* point, for example, there was only one registered land breeze day in June and only one in August. Such pattern can be explained by the fact that during the summer nights the temperature difference between the water surface and the neighbouring land is not high enough to generate a thermal circulation that overlaps the dominant flow due to the major and much more stronger Ocean breeze system. In the cold period, however, the nocturnal temperature differences between the water surface and the neighbouring land tend to be greater and the ocean breeze system is absent, so that land breezes are easy to develop in the banks of Alqueva.

The simulation results for the lake breeze are consistent with data from 2 years observations at two sites on the opposite shores of the Alqueva, recently published by Purificação *et al.* (2021). However, this study suggests that simulations underestimate the occurrence of land breezes.

4 | DISCUSSION

Emergence of a large water reservoir in southwestern Iberia under Mediterranean climate has greatly transformed the local environment. Changes in the weather regime are only a small part of this transformation, however, they are significant for agriculture and people life. The simulation made in the present work revealed many aspects of the lake impact on the meteorological conditions. Although the strongest effects are obviously observed over the water surface, the traces of the impact can be found at distances up to 20 km away from the shores.

The analysis of the lake impact on air temperature showed that the warming effect dominates over the cooling. During the nights, the air warmed by the lake is frequently advected southeastwards following the large-scale circulation. This relatively warm air can reach distances of 20 km in the downwind direction. The air cooled by the reservoir during the daytime also spreads to the land with the dominant wind system. This kind of impact is most powerful during the summer and probably due to the frequent arrival of strong winds linked to the ocean breeze organized at the Iberia peninsular scale. In this case, lake cold air (1–1.2°C) can be found at 5–7 km in the east direction of the Alqueva. Over the water surface, air temperature anomalies varies from −9 to +10°C.

Since the lake impact on the air temperature is spread mainly to the south-east direction, towns to the north and west from the Alqueva are almost unaffected. In the close locations to the east of the reservoir (e.g., Mourão town), daily air temperature has changed significantly: the daily maximum temperature decreased by 0.3–0.6°C while the daily minimum temperature increased on average by 0.5–1.0°C. Hence, we can state that the weather in this location became milder due to the presence of the Alqueva reservoir. On certain days, however, lake impact on maximum and minimum temperature can be much higher, reaching 3°C.

Contrary to the common sense opinion and the feeling of many of the inhabitants, the impact of the reservoir on fog formation appeared to be mostly negative. Throughout the whole TMY, the simulation results suggest a reduction of fog in the nearby area around the reservoir. This is mainly due to a night-time increase of air temperature that suppresses the formation of radiative fogs. However, some cases of the strong Alqueva fogs can be found during the chosen time period. Low-level clouds formed at the reservoir's shore during the afternoon of 19 and 20 of December is an example. On both days, the clouds were developing during 8–10 hr, reached up to 300 m in altitude, and spread up to 60 km north-west. It is possible that such cases may occur more often in 'non-typical' meteorological conditions and could not be traced during the TMY.

The formation of the Alqueva local breeze system was demonstrated in the previous case study (Iakunin

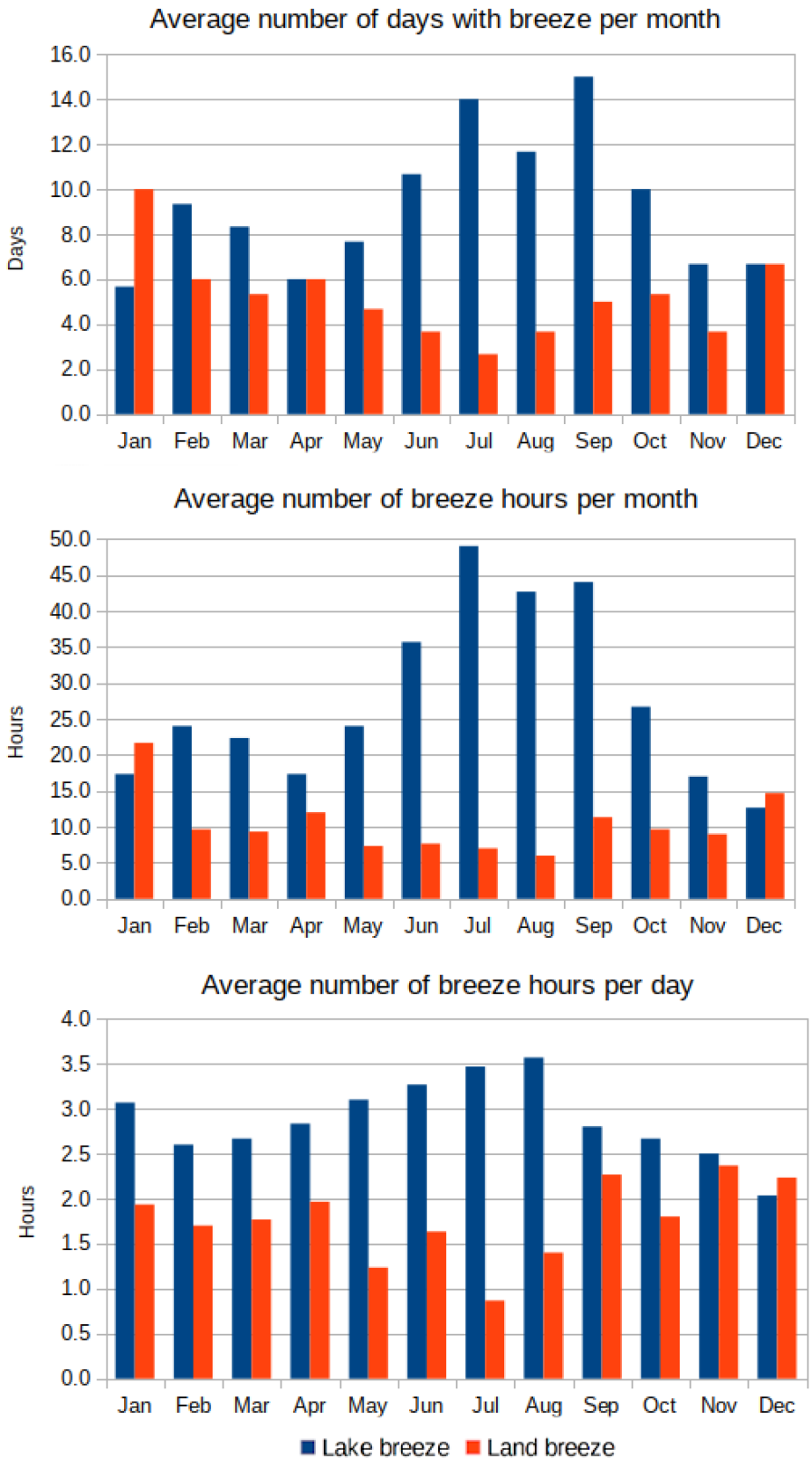

FIGURE 12 Lake and land breeze regime at the Alqueva over the TMY [Colour figure can be viewed at wileyonlinelibrary.com]

et al., 2018). The simulation over the TMY showed the presence of a 'lake breeze season' during June–October. However, even winter months can provide favourable conditions for the lake breeze formation. Land breezes at the Alqueva seem to be less frequent than lake breezes were simulated and observed mostly during the winter

periods. Although the reservoir creates suitable atmospheric conditions (land/water surface thermal contrast) on some summer nights for the formation of land breezes, it cannot be traced due to the stronger large-scale Atlantic breeze system that invades the region in late afternoon and overlaps all local wind circulations.

The numerical experiment that were carried out in the current work demonstrated a success of the chosen approach and method, and, meanwhile, revealed several disadvantages of it. Thus, some atmospheric effects, probably, cannot be featured in the typical meteorological conditions (i.e., during the TMY) and may only appear in non-typical or extreme conditions. A numerical simulation covering the whole life period of the Alqueva reservoir could reveal more characteristic features of its impact, for example, some extreme events of fog or strong breezes. The present study did not investigate the impact of land use change or urbanization increase caused by the reservoir emergence, as the ECOCLIMAP II database used in the model runs does not reflect these changes in the region, which are source of additional effects.

Despite all the limitations, the proposed method for the assessment of the raw impact of the reservoir demonstrates general trends in the local weather changes due to the emergence of the Alqueva and allows to answer the questions posed in the work. The results of this study could be a starting point for a deeper research of the reservoir's impact on climate, or, on the opposite, become a reference for the study of the reservoir's ecosystem response to the climate change.

ACKNOWLEDGEMENTS

The work is co-funded by the European Union through the European Regional Development Fund, included in the COMPETE 2020 (Operational Program Competitiveness and Internationalization) through the ICT project (UID/GEO/04683/2019) with the reference POCI-01-0145-FEDER-007690, the ALOP project (ALT20-03-0145-FEDER-000004), and the TOMAQAPA project (FCT reference PTDC/CTA-MET/29678/2017). Edgar F. M. Abreu acknowledges the support of the FCT (the Portuguese Science and Technology Foundation) through the grant with reference SFRH/BD/136433/2018.

CONFLICT OF INTEREST

The authors declare that they have no conflict of interest.

AUTHOR CONTRIBUTIONS

Edgar Abreu: Data curation; methodology. **Paulo Canhoto:** Methodology; supervision. **Sara Pereira:** Methodology. **Rui Salgado:** Conceptualization; formal analysis; funding acquisition; project administration; resources; supervision; writing-review & editing.

ENDNOTE

[1] All climate data for this paragraph was taken from Portuguese Institute of the Sea and the Atmosphere, http://www.ipma.pt

DATA AVAILABILITY STATEMENT

Current version of the Meso-NH atmospheric model is available for download on the official website http://mesonh.aero.obs-mip.fr/mesonh54/Download.

ORCID

Maksim Iakunin https://orcid.org/0000-0002-8272-2626
Rui Salgado https://orcid.org/0000-0003-1311-6291

REFERENCES

Abreu, E.F.M., Canhoto, P., Prior, V. and Melicio, R. (2018) Solar resource assessment through long-term statistical analysis and typical data generation with different time resolutions using GHI measurements. *Renewable Energy*, 127, 398–411. https://doi.org/10.1016/j.renene.2018.04.068.

Bates, G.T., Giorgi, F. and Hostetler, S.W. (1993) Toward the Simulation of the Effects of the Great Lakes on Regional Climate. *Monthly Weather Review*, 121, 1373–1387. https://doi.org/10.1175/1520-0493(1993)121<1373:TTSOTE>2.0.CO;2.

Bergot T., Lestringant R. (2019) On the Predictability of Radiation Fog Formation in a Mesoscale Model: A Case Study in Heterogeneous Terrain. *Atmosphere*, 10(4), 165. http://dx.doi.org/10.3390/atmos10040165.

Bischoff-Gauß, I., Kalthoff, N. and Fiebig-Wittmaack, M. (2006) The influence of a storage lake in the Arid Elqui Valley in Chile on local climate. *Theoretical and Applied Climatology*, 85, 227–241. https://doi.org/10.1007/s00704-005-0190-8.

Bonan, G.B. (1995) Sensitivity of a GCM simulation to inclusion of inland water surfaces. *Journal of Climate*, 8, 2691–2704. https://doi.org/10.1175/1520-0442(1995)008<2691:SOAGST>2.0.CO;2.

Bougeault, P. and Lacarrere, P. (1989) Parameterization of orography-induced turbulence in a mesobeta–scale model. *Monthly Weather Review*, 117, 1872–1890. https://doi.org/10.1175/1520-0493(1989)117<1872:POOITI>2.0.CO;2.

Bre, F. and Fachinotti, V.D. (2016) Generation of typical meteorological years for the Argentine Littoral Region. *Energy and Buildings*, 129, 432–444. https://doi.org/10.1016/j.enbuild.2016.08.006.

Capecchi, V. and Buizza, R. (2019) Reforecasting the flooding of florence of 4 November 1966 With Global and Regional Ensembles. *Journal of Geophysical Research: Atmospheres*, 124, 3743–3764. https://doi.org/10.1029/2018JD030231.

Chan, A. (2016) Generation of typical meteorological years using genetic algorithm for different energy systems. *Renewable Energy*, 90, 144–151. https://doi.org/10.1016/j.renene.2015.12.052.

Choulga, M., Kourzeneva, E., Zakharova, E. and Doganovsky, A. (2014) Estimation of the mean depth of boreal lakes for use in numerical weather prediction and climate modelling. *Tellus A: Dynamic Meteorology and Oceanography*, 66, 295. https://doi.org/10.3402/tellusa.v66.21295.

Cohard, J.M. and Pinty, J.P. (2000) A comprehensive two-moment warm microphysical bulk scheme. I: Description and tests.

Quarterly Journal of the Royal Meteorological Society, 126, 1815–1842. https://doi.org/10.1002/qj.49712656613.

Cuxart, J., Bougeault, P. and Redelsperger, J.-L. (2000) A turbulence scheme allowing for mesoscale and large-eddy simulations. *Quarterly Journal of the Royal Meteorological Society*, 126, 1–30. https://doi.org/10.1002/qj.49712656202.

Domínguez, A., Martínez-Romero, A., Leite, K.N., Tarjuelo, J.M., de Juan, J.A. and López-Urrea, R. (2013) Combination of typical meteorological year with regulated deficit irrigation to improve the profitability of garlic growing in central Spain. *Agricultural Water Management*, 130, 154–167. https://doi.org/10.1016/j.agwat.2013.08.024.

Eerola, K., Rontu, L., Kourzeneva, E., Homa, K.P. and Duguay, C. (2014) Impact of partly ice-free Lake Ladoga on temperature and cloudiness in an anticyclonic winter situation – a case study using a limited area model. *Tellus A: Dynamic Meteorology and Oceanography*, 66, 929. https://doi.org/10.3402/tellusa.v66.23929.

Ekhtiari N., Grossman-Clarke S., Koch H., Meira de Souza W., Donner R., Volkholz J. (2017) Effects of the Lake Sobradinho Reservoir (Northeastern Brazil) on the Regional Climate. *Climate*, 5(3), 50. http://dx.doi.org/10.3390/cli5030050.

Faroux, S., Kaptué Tchuenté, A.T., Roujean, J.L., Masson, V., Martin, E. and Le Moigne, P. (2013) ECOCLIMAP-II/Europe: a twofold database of ecosystems and surface parameters at 1 km resolution based on satellite information for use in land surface, meteorological and climate models. *Geoscientific Model Development*, 6, 563–582. https://doi.org/10.5194/gmd-6-563-2013.

Fernández, M.D., López, J.C., Baeza, E., Céspedes, A., Meca, D.E. and Bailey, B. (2015) Generation and evaluation of typical meteorological year datasets for greenhouse and external conditions on the Mediterranean coast. *International Journal of Biometeorology*, 59, 1067–1081. https://doi.org/10.1007/s00484-014-0920-7.

Festa, R. and Ratto, C. (1993) Proposal of a numerical procedure to select reference years. *Solar Energy*, 50, 9–17. https://doi.org/10.1016/0038-092X(93)90003-7.

Finkelstein, J. and Schafer, R. (1971) Improved goodness-of-fit tests. *Biometrika*, 58, 641–645. https://doi.org/10.1093/biomet/58.3.641.

Gazela, M. and Mathioulakis, E. (2001) A new method for typical weather data selection to evaluate long-term performance of solar energy systems. *Solar Energy*, 70, 339–348. https://doi.org/10.1016/S0038-092X(00)00151-1.

Haichao, W., Wenling, J., Lahdelma, R., Pinghua, Z. and Shuhui, Z. (2013) Atmospheric environmental impact assessment of a combined district heating system. *Building and Environment*, 64, 200–212. https://doi.org/10.1016/j.buildenv.2013.02.011.

Hall, I., Prairie, R.R., Anderson, H.E. and Boes, E.C. (1978) *Generation of Typical Meteorological Years for 26 SOLMET Stations*. Sandia Laboratories: Sandia Laboratories energy report.

Hogan, R.J. and Bozzo, A. (2018) A flexible and efficient radiation scheme for the ECMWF model. *Journal of Advances in Modeling Earth Systems*, 10, 1990–2008. https://doi.org/10.1029/2018MS001364.

Iakunin, M., Salgado, R. and Potes, M. (2018) Breeze effects at a large artificial lake: summer case study. *Hydrology and Earth System Sciences*, 22, 5191–5210. https://doi.org/10.5194/hess-22-5191-2018.

Iakunin, M., Stepanenko, V., Salgado, R., Potes, M., Penha, A., Novais, M.H. and Rodrigues, G. (2020) Numerical study of the seasonal thermal and gas regimes of the largest artificial reservoir in western Europe using the LAKE 2.0 model. *Geoscientific Model Development*, 13, 3475–3488. https://doi.org/10.5194/gmd-13-3475-2020.

Jarvis, A., Guevara, E., Reuter, H. I., and Nelson, A. D. (2008). Hole - filled SRTM for the globe: version 4: data grid, published by CGIAR-CSI on August 19, 2008.

Jiménez, M.A., Cuxart, J. and Martínez-Villagrasa, D. (2019) Influence of a valley exit jet on the nocturnal atmospheric boundary layer at the foothills of the Pyrenees. *Quarterly Journal of the Royal Meteorological Society*, 145, 356–375. https://doi.org/10.1002/qj.3437.

Lac, C., Chaboureau, J.-P., Masson, V., Pinty, J.P., Tulet, P., Escobar, J., Leriche, M., Barthe, C., Aouizerats, B., Augros, C., Aumond, P., Auguste, F., Bechtold, P., Berthet, S., Bieilli, S., Bosseur, F., Caumont, O., Cohard, J.-M., Colin, J., Couvreux, F., Cuxart, J., Delautier, G., Dauhut, T., Ducrocq, V., Filippi, J.-B., Gazen, D., Geoffroy, O., Gheusi, F., Honnert, R., Lafore, J.-P., Lebeaupin Brossier, C., Libois, Q., Lunet, T., Mari, C., Maric, T., Mascart, P., Mogé, M., Molinié, G., Nuissier, O., Pantillon, F., Peyrillé, P., Pergaud, J., Perraud, E., Pianezze, J., Redelsperger, J.-L., Ricard, D., Richard, E., Riette, S., Rodier, Q., Schoetter, R., Seyfried, L., Stein, J., Suhre, K., Thouron, O., Turner, S., Verrelle, A., Vié, B., Visentin, F., Vionnet, V. and Wautelet, P. (2018) Overview of the Meso-NH model version 5.4 and its applications. *Geoscientific Model Development Discussions*, 2018, 1–66. https://doi.org/10.5194/gmd-2017-297.

Le Moigne, P., Colin, J. and Decharme, B. (2016) Impact of lake surface temperatures simulated by the FLake scheme in the CNRM-CM5 climate model. *Tellus A: Dynamic Meteorology and Oceanography*, 68, 31274. https://doi.org/10.3402/tellusa.v68.31274.

Lopes, F., Silva, H.G., Salgado, R., Potes, M., Nicoll, K.A. and Harrison, R.G. (2016) Atmospheric electrical field measurements near a fresh water reservoir and the formation of the lake breeze. *Tellus A: Dynamic Meteorology and Oceanography*, 68, 31592. https://doi.org/10.3402/tellusa.v68.31592.

Lunet, L., Lac, C., Auguste, F., Visentin, F., Masson, V. and Escobar, J. (2017) Combination of WENO and Explicit Runge–Kutta Methods for Wind Transport in the Meso-NH Model. *Monthly Weather Review*, 145, 3817–3838. https://doi.org/10.1175/MWR-D-16-0343.1.

Marion, W. and Urban, K. (1995). *User's manual for TMY2s typical meteorological years: derived from the 1961–1990 national solar radiation data base*. Technical report., https://doi.org/10.2172/87130.

Marsigli, C., Montani, A. and Paccagnella, T. (2014) Provision of boundary conditions for a convection-permitting ensemble: comparison of two different approaches. *Nonlinear Processes in Geophysics*, 21, 393–403. https://doi.org/10.5194/npg-21-393-2014.

Martínez-Romero, A., Domínguez, A. and Landeras, G. (2019) Regulated deficit irrigation strategies for different potato cultivars under continental Mediterranean-Atlantic conditions. *Agricultural Water Management*, 216, 164–176. https://doi.org/10.1016/j.agwat.2019.01.030.

Masson, V. (2000) A physically-based scheme for the urban energy budget in atmospheric models. *Boundary-Layer Meteorology*, 94, 357–397. https://doi.org/10.1023/A:1002463829265.

Masson, V., Le Moigne, P., Martin, E., Faroux, S., Alias, A., Alkama, R., Belamari, S., Barbu, A., Boone, A., Bouyssel, F., Brousseau, P., Brun, E., Calvet, J.-C., Carrer, D., Decharme, B., Delire, C., Donier, S., Essaouini, K., Gibelin, A.-L., Giordani, H., Habets, F., Jidane, M., Kerdraon, G., Kourzeneva, E., Lafaysse, M., Lafont, S., Lebeaupin Brossier, C., Lemonsu, A., Mahfouf, J.-F., Marguinaud, P., Mokhtari, M., Morin, S., Pigeon, G., Salgado, R., Seity, Y., Taillefer, F., Tanguy, G., Tulet, P., Vincendon, B., Vionnet, V. and Voldoire, A. (2013) The SURFEXv7.2 land and ocean surface platform for coupled or offline simulation of earth surface variables and fluxes. *Geoscientific Model Development*, 6, 929–960. https://doi.org/10.5194/gmd-6-929-2013.

Mironov, D. (2008). *Parameterization of lakes in numerical weather prediction. Description of a lake model. COSMO Technical Report*. Deutscher Wetterdienst, 11, pp. 41.

Muñoz, S.J. (2019). ERA5-Land monthly averaged data from 1981 to present. *Copernicus Climate Change Service (C3S) Climate Data Store (CDS)*. [Accessed 12th January 2020], https://doi.org/10.24381/cds.68d2bb3.

Nachtergaele, F., Van Velthuizen, H., Verelst, L., Batjes, N., Dijkshoorn, K., Van Engelen, V., Fischer, G., Jones, A., Montanarella, L., Petri, M. and Prieler, S. (2008) *Harmonized world soil database*. Rome: FAO.

Noilhan, J. and Mahfouf, J.F. (1996) The ISBA land surface parameterisation scheme. *Global and Planetary Change*, 13, 145–159. https://doi.org/10.1016/0921-8181(95)00043-7.

Notaro, M., Zarrin, A., Vavrus, S. and Bennington, V. (2013) Simulation of heavy lake-effect snowstorms across the Great Lakes Basin by RegCM4: synoptic climatology and variability. *Monthly Weather Review*, 141, 1990–2014. https://doi.org/10.1175/MWR-D-11-00369.1.

Novais M.H., Penha A.M., Morales E.A., Potes M., Salgado R., Morais M. (2019) Vertical distribution of benthic diatoms in a large reservoir (Alqueva, Southern Portugal) during thermal stratification. *Science of The Total Environment*, 659 1242–1255. http://dx.doi.org/10.1016/j.scitotenv.2018.12.251.

Penha, A.M., Chambel, A., Murteira, M. and Morais, M. (2016) Influence of different land uses on groundwater quality in southern Portugal. *Environmental Earth Sciences*, 75, 622. https://doi.org/10.1007/s12665-015-5038-7.

Pergaud, J., Masson, V., Malardel, S. and Couvreux, F. (2009) A parameterization of dry thermals and shallow cumuli for mesoscale numerical weather prediction. *Boundary-Layer Meteorology*, 132, 83. https://doi.org/10.1007/s10546-009-9388-0.

Pinty, J. P. and Jabouille, P. (1998) A mixed-phase cloud parameterization for use in mesoscale non-hydrostatic model: simulations of a squall line and of orographic precipitations. *Proceedings of the AMS Conference on Cloud Physics*. Everett, WA: American Meteorological Society, pp. 217–220.

Pissimanis, D., Karras, G., Notaridou, V. and Gavra, K. (1988) The generation of a "typical meteorological year" for the city of Athens. *Solar Energy*, 40, 405–411. https://doi.org/10.1016/0038-092X(88)90095-3.

Policarpo, C., Salgado, R. and Costa, M.J. (2017) Numerical Simulations of Fog Events in Southern Portugal. *Advances in Meteorology*, 16, 2017.

Potes, M., Costa, M.J. and Salgado, R. (2012) Satellite remote sensing of water turbidity in Alqueva reservoir and implications on lake modelling. *Hydrol. Earth Syst. Sci.*, 16, 1623–1633. https://doi.org/10.5194/hess-16-1623-2012.

Potes, M., Rodrigues, G., Penha, A., Novais, M.H., Costa, M.J., Salgado, R. and Morais, M. (2018) Use of Sentinel 2-MSI for water quality monitoring at Alqueva reservoir, Portugal. *Proceedings of the International Association of Hydrological Sciences*, 380, 73–79. https://doi.org/10.5194/piahs-380-73-2018.

Potes, M., Salgado, R., Costa, M.J., Morais, M., Bortoli, D., Kostadinov, I. and Mammarella, I. (2017) Lake–atmosphere interactions at Alqueva reservoir: a case study in the summer of 2014. *Tellus A: Dynamic Meteorology and Oceanography*, 69, 1272787. https://doi.org/10.1080/16000870.2016.1272787.

Purificação C., Potes M., Rodrigues G., Salgado R., Costa M.J. (2021) Lake and Land Breezes at a Mediterranean Artificial Lake: Observations in Alqueva Reservoir, Portugal. *Atmosphere*, 12(5), 535. http://dx.doi.org/10.3390/atmos12050535.

Pusat, S., Ekmekçi, M. and Akkoyunlu, M. (2015) Generation of a typical meteorological year for different climates of Turkey. *Renewable Energy*, 75, 144–151. https://doi.org/10.1016/j.renene.2014.09.039.

Reinares Martínez I., Chaboureau J.-P., Handwerker J. (2020) Warm Rain in Southern West Africa: A Case Study at Savè. *Atmosphere*, 11(3), 298. http://dx.doi.org/10.3390/atmos11030298.

Rodrigues G., Potes M., Costa M.J., Novais M.H., Penha A.M., Salgado R., Morais M.M. (2020) Temporal and Spatial Variations of Secchi Depth and Diffuse Attenuation Coefficient from Sentinel-2 MSI over a Large Reservoir. *Remote Sensing*, 12(5), 768. http://dx.doi.org/10.3390/rs12050768.

Salgado, R. and Le Moigne, P. (2010) Coupling of the FLake model to the Surfex externalized surface model. *Boreal Environment Research*, 15, 231–244.

Samuelsson, P., Kourzeneva, E. and Mironov, D. (2010) The impact of lakes on the European climate as simulated by a regional climate model. *Boreal Environment Research*, 15, 113–129, Available at: http://www.borenv.net/BER/pdfs/ber15/ber15-113.pdf.

Scott, R.W. and Huff, F.A. (1996) Impacts of the Great Lakes on regional climate conditions. *Journal of Great Lakes Research*, 22, 845–863. https://doi.org/10.1016/S0380-1330(96)71006-7.

Segal, M., Leuthold, M., Arritt, R.W., Anderson, C. and Shen, L. (1997) Small lake daytime breezes: some observational and conceptual evaluations. *Bulletin of the American Meteorological Society*, 78, 1135–1147. https://doi.org/10.1175/1520-0477(1997)078<1135:SLDBSO>2.0.CO;2.

Silva, A., De Lima, I., Santo, F. and Pires, V. (2014) Assessing changes in drought and wetness episodes in drainage basins using the Standardized Precipitation Index. *Bodenkultur*, 65(3–4), 31–37.

Thiery, W., Martynov, A., Darchambeau, F., Descy, J.-P., Plisnier, P.-D., Sushama, L. and van Lipzig, N.P.M. (2014) Understanding the performance of the FLake model over two African Great Lakes. *Geoscientific Model Development*, 7, 317–337. https://doi.org/10.5194/gmd-7-317-2014.

Tomaz, A., Patanita, M., Guerreiro, I., Boteta, L. and Palma, J.F. (2017) Water use and productivity of maize-based cropping

systems in the Alqueva Region (Portugal). *Cereal Research Communications*, 45, 1–11. https://doi.org/10.1556/0806.45.2017.036.

Verrelle, A., Ricard, D. and Lac, C. (2015) Sensitivity of high-resolution idealized simulations of thunderstorms to horizontal resolution and turbulence parametrization. *Quarterly Journal of the Royal Meteorological Society*, 141, 433–448. https://doi.org/10.1002/qj.2363.

Wilcox, S. and Marion, W. (2008). *Users manual for TMY3 data sets*, https://doi.org/10.2172/928611.

How to cite this article: Iakunin, M., Abreu, E. F. M., Canhoto, P., Pereira, S., & Salgado, R. (2022). Impact of a large artificial lake on regional climate: A typical meteorological year Meso-NH simulation results. *International Journal of Climatology*, *42*(2), 1231–1252. https://doi.org/10.1002/joc.7299